

Utah State University

DigitalCommons@USU

Chemistry and Biochemistry Student Research

Chemistry and Biochemistry Student Works

4-19-2017

Properties of Flavonol-based PhotoCORM in Aqueous Buffered Solutions: Influence of Metal Ions, Surfactants and Proteins on Visible Light-induced CO Release

Marina Popova
Utah State University

Tatiana Soboleva
Utah State University, tatiana.soboleva@aggiemail.usu.edu

Atta M. Arif
Utah State University

Lisa M. Berreau
Utah State University

Follow this and additional works at: https://digitalcommons.usu.edu/chem_stures

Recommended Citation

Marina Popova, Tatiana Soboleva, Atta M. Arif, and Lisa M. Berreau, "Properties of Flavonol-based PhotoCORM in Aqueous Buffered Solutions: Influence of Metal Ions, Surfactants and Proteins on Visible Light-induced CO Release," *RSC Adv.*, 7, 21997-22007.

This Article is brought to you for free and open access by the Chemistry and Biochemistry Student Works at DigitalCommons@USU. It has been accepted for inclusion in Chemistry and Biochemistry Student Research by an authorized administrator of DigitalCommons@USU. For more information, please contact digitalcommons@usu.edu.



Cite this: *RSC Adv.*, 2017, 7, 21997

Properties of a flavonol-based photoCORM in aqueous buffered solutions: influence of metal ions, surfactants and proteins on visible light-induced CO release†

Marina Popova,^a Tatiana Soboleva,^a Atta M. Arif^b and Lisa M. Berreau ^{*a}

The properties of the extended flavonol 3-hydroxy-2-phenyl-benzo[*g*]chromen-4-one (**2a**) in DMSO : aqueous buffer solutions at pH = 7.4, including in the presence of metal ions, surfactants and serum albumin proteins, have been examined. Absorption and emission spectral studies of **2a** in 1 : 1 DMSO : PBS buffer (pH = 7.4) indicate that a mixture of neutral and anionic forms of the flavonol are present. Notably, in 1 : 1 DMSO : TRIS buffer (pH = 7.4) only the neutral form of the flavonol is present. These results indicate that the nature of the buffer influences the acid/base equilibrium properties of **2a**. Introduction of a Zn(II) complex of **2a**⁻ to a 1 : 1 DMSO : aqueous buffer (TRIS or PBS, pH = 7.4) solution produces absorption and emission spectral features consistent with the presence of a mixture of neutral **2a** along with Zn(II)-coordinated or free **2a**⁻. The nature of the anionic species present depends on the buffer composition. PBS buffered solutions (pH = 7.4) containing the surfactants CTAB or SDS enable **2a** to be solubilized at a much lower percentage of DMSO (3.3–4.0%). Solutions containing the cationic surfactant CTAB include a mixture of **2a** and **2a**⁻ whereas only the neutral flavonol is present in SDS-containing buffered solution. Compound **2a** is also solubilized in TRIS buffer solutions at low concentrations of DMSO (3.3%, pH = 7.4) in the presence of serum albumin proteins. Stern–Volmer analysis of the quenching of the inherent protein fluorescence indicates static binding of **2a** to the proteins. The binding constant for this interaction is lower than that found for naturally-occurring flavonols (quercetin or morin) or 3-hydroxyflavone. Compound **2a** binds to Site I of bovine and human serum albumin proteins as indicated by competition studies with warfarin and ibuprofen, as well as by docking investigations. The quantum yield for CO release from **2a** ($\lambda_{\text{irr}} = 419 \text{ nm}$) under aqueous conditions ranges from 0.0006(3) when the compound is bound to bovine serum albumin to 0.017(1) when present as a zinc complex in a 1 : 1 DMSO : H₂O solution. Overall, the results of these studies demonstrate that **2a** is a predictable visible light-induced CO release compound under a variety of aqueous conditions, including in the presence of proteins.

Received 4th March 2017
Accepted 10th April 2017

DOI: 10.1039/c7ra02653f

rsc.li/rsc-advances

Introduction

Carbon monoxide (CO) is generated in humans *via* the oxidative degradation of heme, which is catalyzed by heme oxygenase enzymes.¹ The discovery of beneficial health effects associated with the delivery of small amounts of CO, including anti-inflammatory, anti-apoptotic, and anti-proliferative effects, as well as the promotion of vasodilation and protection of tissues against reperfusion injury, has led to investigations of the

possible use of CO as a therapeutic.^{2–8} Several clinical trials are currently in progress involving the use of inhaled carbon monoxide.^{9–14} A challenge in using inhaled CO as a therapeutic is that it does not enable the delivery of controlled amounts of CO to specific targets and diffusion into tissues is unpredictable. As an approach toward introducing controlled amounts of CO, several research labs have worked on the development of CO-releasing molecules (CORMs).^{15,16} The most widely investigated CORMs to date are metal carbonyl complexes,¹⁷ with CORM-1 and CORM-3 (Fig. 1(top)) having been employed in a variety of biological investigations. Metal carbonyl-based CORMs release CO either spontaneously *via* ligand exchange, or *via* triggering with light (photoCORMs),^{18–25} enzyme activity,^{26–29} or magnetic heating^{30–32} (Fig. 1). A drawback of the use of metal carbonyl complexes as CORMs is the possible (or perceived) toxicity of the residual low-valent metal fragment

^aDepartment of Chemistry & Biochemistry, Utah State University, 0300 Old Main Hill, Logan, UT 84322-0300, USA. E-mail: lisa.berreau@usu.edu^bDepartment of Chemistry, University of Utah, 315 S. 1400 E., Salt Lake City, UT 84112-0850, USA

† Electronic supplementary information (ESI) available. CCDC 1523782. For ESI and crystallographic data in CIF or other electronic format see DOI: 10.1039/c7ra02653f



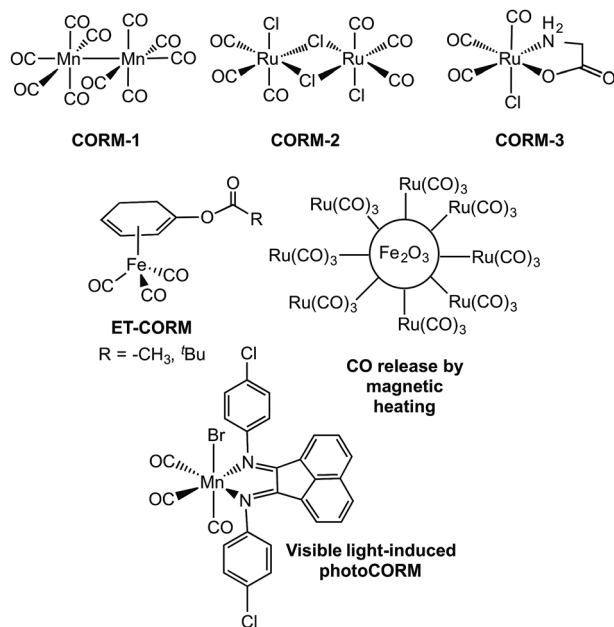


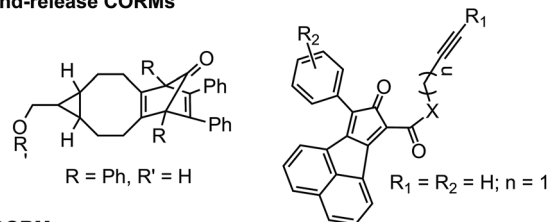
Fig. 1 Examples of metal carbonyl-based CORMs.^{17,20,28,30}

remaining following CO release. Additionally, little is currently known in terms of the reactivity of metal carbonyl-based CORMs with other biomolecules. It was only after CORM-3 had been used in a several biological studies that the active form for CO-release *in vivo* was determined to likely be a protein-bound Ru(CO)₂ species.^{33,34} In general, although many metal carbonyl species have been demonstrated to be CORMs and to enable CO release both *in vitro* and in cellular environments, very few have been studied with regard to their interactions with biological molecules, such as proteins.^{35,36} These interactions could dramatically affect the CO-release reactivity.

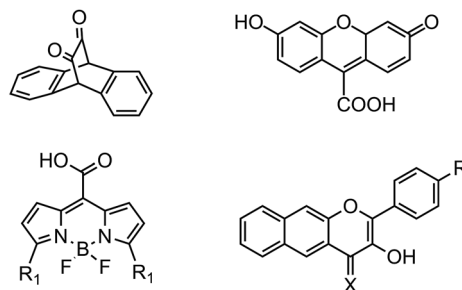
Metal-free CORMs^{37,38} and photoCORMs^{39–42} (Fig. 2) have recently emerged as alternatives to metal carbonyl-based CO-releasing molecules. Of the structural frameworks reported thus far for metal-free photoCORMs, the BODIPY and extended flavonol motifs (Fig. 2) are notable in that they can be tuned to enable the use of low energy visible light (>575 nm) to induce CO release, which is important for use in biological environments. The CO release unit in **1a/1b** is a carboxyl moiety whereas the extended flavonol motif in **2a–d** contains a pyrone ring that is similar to naturally occurring flavonols (*e.g.*, quercetin), which are known to undergo enzyme-catalyzed CO release.⁴³ The visible light-induced CO release reaction involving **1a** or **1b** proceeds in high yield (87–92%) only under anaerobic conditions, with the yield of CO under aerobic conditions dropping to 42–44%.³⁹ Visible light-induced carbon monoxide release from **2a–c** requires the presence of O₂ for a quantitative, dioxygenase-type reaction to produce an *O*-benzoylsalicylic acid product (**3a**, Scheme 1). Complex **2d** exhibits both aerobic and anaerobic visible light-induced quantitative CO release reactivity.⁴²

Development of an understanding of the properties of metal-free CO-releasing photoCORM frameworks in aqueous buffered solutions and in the presence of biomolecules is essential

Click-and-release CORMs



PhotoCORMs



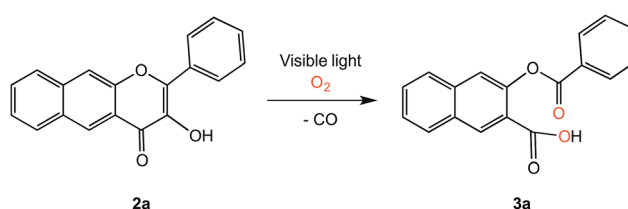
- 1a:** R₁ = -CH₃
1b: R₁ = -CH=CH-C₆H₄-O(CH₂CH₂O)₃CH₃

- 2a:** X = O, R = H
2b: X = O, R = NEt₂
2c: X = S, R = H
2d: X = S, R = NEt₂

Fig. 2 Metal-free CORMs and photoCORMs reported to date.^{36–41}

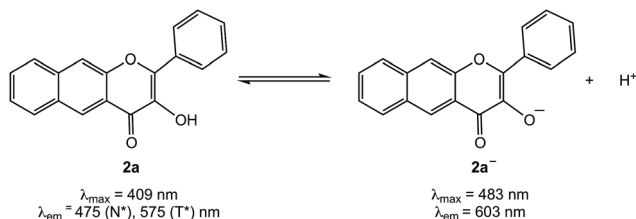
toward the further development of these motifs as potential biological tools and therapeutics. Klán and coworkers have reported that at pH = 7.4 in PBS buffer, **1a** and **1b** exist as monoanions, with a deprotonated carboxyl group (pK_a = 3.0 ± 0.2).³⁹ Under anaerobic conditions in PBS (pH = 7.4) visible light-induced CO release occurs from **1a** and **1b** with quantum yields of 1.2(4) × 10⁻⁴ and 1.2(4) × 10⁻⁵, respectively. It is currently unknown how a biological environment, including the presence of proteins, will affect these values. The organic products in these CO release reactions also remain only partially characterized.

We have previously reported the visible light-induced CO release reactivity of **2a–d**⁴² and zinc complexes of these flavonols in organic solvent (acetonitrile).⁴⁴ All exhibit quantitative CO release under aerobic conditions. The quantum yields for these reactions are significantly affected by the presence of a neutral *versus* anionic form of the flavonol. Specifically, for **2a** the quantum yield for CO release in CH₃CN is 0.007(3) whereas for zinc complex of **2a**⁻ it is 0.651(2), a >90-fold increase.^{42,44} Experimental and computational studies of 3-hydroxyflavone (3-HfH) indicate that the pK_a for this compound is ~8.5 in aqueous solution.⁴⁵ In this contribution, we examine the



Scheme 1 Visible light-induced CO release reaction of **2a**.





Scheme 2 Acid/base equilibrium of 2a.

aqueous solution chemistry of **2a** at pH = 7.4 in buffered solutions that include metal ions, surfactants or serum albumin proteins. Our results indicate that the components of the aqueous buffered environment affect the **2a/2a⁻** equilibrium (Scheme 2) and modestly influence the quantum yield for CO release. Our studies reveal that **2a** is a reliable CO release motif under a variety of aqueous buffered conditions. Combined with its straight-forward preparation, moderate toxicity, and the non-toxic nature of the *O*-benzoylsalicylate product (**3a**) remaining following CO release, **2a** exhibits many features desirable in a photoCORM motif to be further developed for biomedical applications.

Experimental

Reagents

Compound **2a** was prepared according to the literature procedure.⁴² All reagents were used as received unless otherwise noted. Cetrimonium bromide (CTAB) was purchased from TCI. Sodium dodecylsulfate (SDS) was purchased from Acros Organics. Bovine serum albumin (BSA, heat shock fraction) and human serum albumin (HAS, lyophilized powder, ≥97%) were purchased from Sigma Aldrich. Warfarin was purchased from Cayman Chemicals Company. Ibuprofen was purchased from Alfa Aesar. Double-distilled or distilled water was used in all experiments.

Instrumentation

¹H and ¹³C NMR spectra were collected using a Bruker Avance III HD Ascend-500 spectrometer. UV-vis spectra were recorded at ambient temperature using a Cary 50Bio or a Hewlett-Packard 8453A diode array spectrophotometer. Fluorescence emission spectra were recorded using a Shimadzu RF-530XPC spectrometer using 1.0 cm quartz cells. The excitation and emission slit widths were set at 3.0 nm. IR spectra were collected using a Shimadzu FTIR-8400 spectrometer. Mass spectral data were collected at the Mass Spectrometry Facility, University of California, Riverside. Elemental analyses were performed by Robertson Microlit Laboratory, Ledgewood, NJ. A Rayonet photoreactor equipped with RPR-419 lamps was used for all photochemical reactions. Quantum yields were determined as previously described using potassium ferrioxalate as a standard to measure photon flux.^{46–48}

[(bpy)Zn(2a⁻)]ClO₄ (**4**)

Zn(ClO₄)₂·6H₂O (50 mg, 0.13 mmol) dissolved in 1 ml of methanol was added to 2,2'-bipyridine (21 mg, 0.13 mmol) in

1 ml of methanol. The resulting mixture was added to a mixture of **2a** (39 mg, 0.13 mmol) and Me₄NOH·5H₂O (24 mg, 0.13 mmol) in methanol (2 mL). The reaction mixture was stirred at room temperature for 3 hours. The resulting solution was divided into three parts and solvent was removed under reduced pressure. The remaining residue was dissolved in CH₂Cl₂, the solution was filtered through Celite plug, and the solvent was removed under vacuum. The product was recrystallized from ACN/Et₂O, which resulted in the deposition of X-ray quality crystals (45%). IR (KBr, cm⁻¹) 1100 (ν_{ClO₄}), 623 (ν_{ClO₄}); UV-vis (DMSO, nm) (ε, M⁻¹ cm⁻¹) 378 (3100), 479 (15 100); ESI/APCI MS (positive ion): *m/z* calculated for C₂₉H₁₉N₂O₃Zn: 507.0722 [M-ClO₄]⁺, found: 507.0699; elemental analysis calc. for C₂₉H₁₉N₂O₇-ClZn·0.5H₂O: C, 56.42%; H, 3.27%; N, 4.61%. Found: C 56.31; H, 2.85; N, 4.60.

X-ray crystallography

A translucent light orange plate-like crystal of **4** of approximate dimensions 0.140 mm × 0.168 mm × 0.392 mm was mounted using a viscous oil. Data were collected using a Nonius Kappa CCD diffractometer (Mo Kα, λ = 0.71073 Å). A total of 2079 frames were collected and subsequently integrated with the Bruker SAINT software package using a narrow-frame algorithm. The integration of the data using a monoclinic unit cell yielded a total of 51 427 reflections to a maximum θ angle of 30.03° (0.71 Å resolution), of which 7184 were independent (average redundancy 7.159, completeness = 99.8%, R_{int} = 2.75%, R_{sig} = 1.73%) and 6280 (87.42%) were greater than 2σ(F²). The final cell constants of *a* = 8.2518(2) Å, *b* = 14.8377(4) Å, *c* = 20.0844(6) Å, β = 92.219(2), volume = 2457.24(12) Å³, are based upon the refinement of the XYZ-centroids of reflections above 20 σ(*I*). Data were corrected for absorption effects using the multi-scan method (SADABS). The calculated minimum and maximum transmission coefficients (based on crystal size) are 0.6600 and 0.8540, respectively.

The structure of **4** was solved and refined using the Bruker SHELXTL Software Package, using the space group *P2₁n* with *Z* = 4 for the formula unit C₂₉H₁₉ClN₂O₇Zn. The final anisotropic full-matrix least-squares refinement on *F*² with 370 variables converged at R₁ = 3.18%, for the observed data and wR₂ = 8.97%. The goodness-of-fit was 1.062. The largest peak in the final difference electron density was 1.263 e⁻ Å⁻³ with an RMS deviation of 0.066 e⁻ Å⁻³. On the basis of the final model, the calculated density was 1.644 g cm⁻³ and F(000), 1240 e⁻. The structure was deposited in the Cambridge Crystallographic Database (CCDC 1523782).

Buffer preparation

TRIS (0.05 M) at pH = 7.4 was prepared using a mixture of TRIS-HCl and TRIS-base. Sodium chloride (0.1 M) was added to maintain ionic strength. Phosphate buffered saline (PBS) was prepared containing 140 mM NaCl, 3 mM KCl, and 10 mM phosphate and was adjusted to pH = 7.4 using aqueous HCl.



Solution studies of 2a in the presence of CTAB and SDS

Experiments were performed in PBS : DMSO (96.7 : 3.3% v:v, pH = 7.4). The absorption and emission properties of 2a were evaluated in the presence of varying amounts of CTAB or SDS.

Solution studies of 2a in the presence of bovine or human serum albumin

Emission spectra of solutions of 2a (1.4×10^{-6} M) in TRIS : DMSO (96 : 4% v:v, pH = 7.4) were collected from 410 to 800 nm in the presence of varying amounts of bovine or human serum albumin (1 : 0 to 1 : 40). The excitation wavelength was 408 nm, which corresponds to the absorption maximum of 2a.

Serum albumin binding studies

Binding studies of 2a to bovine or human serum albumin were performed using tryptophan fluorescence quenching experiments in TRIS : DMSO (96 : 4% v:v, pH = 7.4). The excitation wavelengths used for BSA and HSA were 282 and 285 nm, respectively. Emission spectra were recorded from 300 to 600 nm. The maximum emission intensities at 340 nm were used to calculate binding constants and to determine the number of binding sites.

Molecular docking

Studies were performed using AutoDock Vina 1.1.2 software.⁴⁹ The crystal structure of BSA was downloaded from the RSCB Protein Data Bank (PDB entry code 3V03). The X-ray crystallographically determined structure of 2a⁴² was converted to pdbqt format with MGLTools for use as an input file for AutoDock Vina. A structure of the *O*-benzoylsalicylic acid CO release product 3a was energy minimized using Chem 3D (MM2 force field) and saved in pdbqt format using MGLTools for input into AutoDock Vina. A semi-flexible docking procedure was performed wherein BSA was kept rigid and stationary and was assigned with polar hydrogen atoms. Compound 2a with two rotatable bonds and 3a with five rotatable bonds were allowed to be flexible as they were docked into the protein. A grid box with dimensions $60 \times 68 \times 68$ points with the spacing of 1.0 Å was used to accommodate the ligands to move freely during each docking run. The lowest energy docked conformations identified for 2a and 3a with BSA were visualized using Pymol.

Independent synthesis of 3-(benzoyloxy)-2-naphthoic acid (3a)

3-Hydroxy-2-naphthoic acid, (0.50 g, 2.7 mmol) in 3 ml dry diethyl ether was mixed with pyridine (0.58 ml, 7.2 mmol). The resulting mixture was cooled in an ice bath and a solution of benzoyl chloride (0.31 ml, 2.7 mmol) in diethyl ether (2 mL) was added. The reaction mixture was warmed to room temperature and then stirred for 1 hour. H₂O (10 ml) was then added. The solution was acidified with 2 M HCl until pH ~4 was obtained. The mixed aqueous/organic mixture was then extracted using chloroform (3 × 15 ml). The organic fractions were combined, dried over Na₂SO₄, the solution was filtered, and the solvent was removed from the filtrate under reduced pressure. The product was purified by column chromatography using hexanes : ethyl

acetate (1 : 1) as the eluent. 3-(Benzoyloxy)-2-naphthoic acid (3a) was obtained as colorless needles (0.20 g, 25%) following removal of solvent. The ¹H NMR features of the product in CD₃CN matched with those previously reported.⁴² ¹H NMR (500 MHz, CD₃OD) δ ppm 8.66 (s, 1H), 8.23 (d, *J* = 9 Hz, 2H), 8.05 (d, *J* = 9.5 Hz, 1H), 7.93 (d, *J* = 9 Hz, 1H), 7.73 (s, 1H), 7.69 (t, *J* = 7.5 Hz, 1H), 7.65 (t, *J* = 7.5 Hz, 1H), 7.56 (m, 3H); ¹³C{¹H} NMR (125 MHz, CD₃OD) δ 169.4, 169.0, 149.9, 138.5, 136.2, 136.1, 133.6, 132.7, 132.6, 131.5, 131.4, 131.1, 129.8, 129.3, 125.9, 123.6 ppm (16 signals expected and observed); IR (KBr, cm⁻¹) 1743 ($\nu_{C=O}$); ESI/APCI MS (negative ion): *m/z* calculated for C₁₈H₁₂O₄: 291.0657, found: 291.0674. m.p. 173–175 °C.

Results

Properties of 2a in 1 : 1 DMSO : aqueous buffer at pH = 7.4

When dissolved in 1 : 1 DMSO : Tris buffer at pH 7.4, compound 2a exhibits features consistent with the presence of the neutral flavonol (Fig. 3). Specifically, an absorption band with a maximum at approximately ~409 nm is similar to that observed for the compound in CH₃CN and 1 : 1 DMSO : H₂O.⁴² When 2a is dissolved in 1 : 1 DMSO : PBS buffer at pH 7.4 (Fig. 3), an absorption feature at ~480 nm is also present. This red-shifted band is consistent with the presence of the flavonolato anion (2a⁻) based on comparison to spectroscopic features of Zn(II) complexes of 2a⁻.⁴⁴ The same 480 nm band is present when 2a is dissolved in 1 : 1 DMSO : H₂O to which two equivalents of sodium hydroxide has been added (Fig. S1(a)†).

Fluorescence spectra (λ_{ex} = 410 and 480 nm) of 1 : 1 DMSO : buffer solutions (pH = 7.4) of 2a provide additional evidence for the presence of neutral and anionic forms of 2a under various conditions. When excited at 410 nm, solutions of 2a in 1 : 1 DMSO : H₂O, DMSO : TRIS and 1 : 1 DMSO : PBS at pH = 7.4 exhibit two emission bands at ~475 and ~580 nm (Fig. 4), respectively. These emissions are from the normal (N*) and tautomeric (T*) excited state forms of 2a.⁵⁰ The T* form is

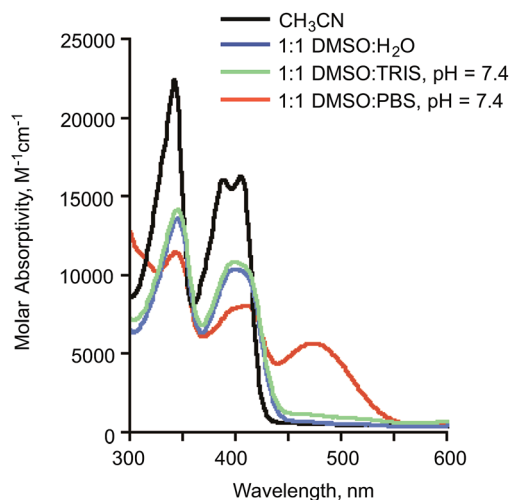


Fig. 3 Absorbance spectra of 2a (0.10 mM) in various solution environments. The ~480 nm absorption feature present in 1 : 1 DMSO : PBS at pH 7.4 is associated with the presence of 2a⁻.



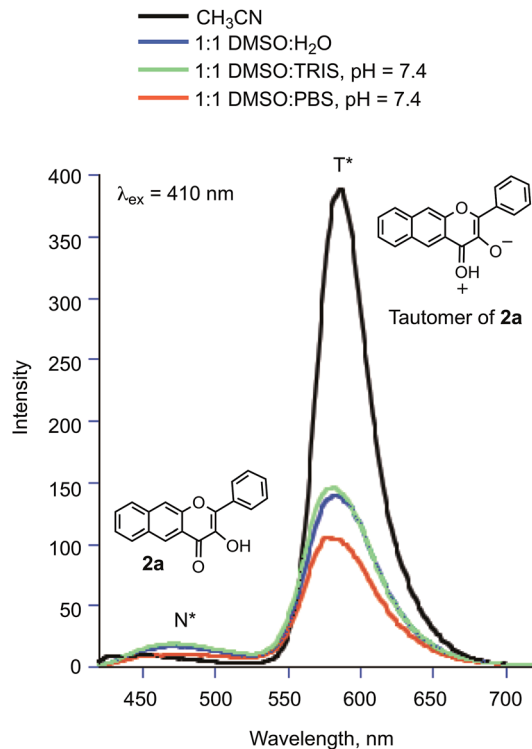


Fig. 4 Emission spectra ($\lambda_{\text{ex}} = 410 \text{ nm}$) of solutions of **2a** (0.10 mM).

the result of excited state proton transfer (ESPT) within the flavonol and formation of the pyrylium ion (Fig. 4). The intensity of the T^* emission is lower than that exhibited by **2a** in organic solvent (CH_3CN) due to the availability of additional non-radiative pathways in the hydrogen bonding aqueous solutions which results in quenching of the excited state.⁵¹ The emission maximum in aqueous environments is also slightly blue-shifted relative to the spectrum of **2a** in CH_3CN . Excitation of the same solutions at 480 nm produced an emission at $\sim 603 \text{ nm}$ in the solution of **2a** in 1 : 1 DMSO : PBS buffer. A 1 : 1 DMSO : H_2O solution containing two equivalents of sodium hydroxide gives a similar emission feature (Fig. S1(c)†) providing evidence that this emission is associated with $2a^-$.

Zinc complex

To gain insight into the properties of $2a^-$ in aqueous buffer in the presence of a divalent metal ion, we have prepared and characterized $[(\text{bpy})\text{Zn}(2a^-)]\text{ClO}_4$ (**4**) and performed spectroscopic studies of this complex. In the solid state, **4** exhibits a binuclear structure (Fig. 6(a)) with the deprotonated oxygen atom of each flavonolato ligand bridging between two zinc centers. This coordination motif is similar to that found in $[(\text{bpy})\text{Zn}(3\text{-Hfl})]\text{ClO}_4$ (3-Hfl = 3-hydroxyflavonolato anion).⁵² ESI APCI mass spectral studies of **4** in wet CH_3CN (Fig. S2†) indicate that the mononuclear $[(\text{bpy})\text{Zn}(2a^-)]^+$ ion is present indicating breakup of the dimer in solution. Additionally, species resulting from ligand exchange (e.g., $[(\text{bpy})_2\text{Zn}(\text{ClO}_4)]^+$ and $[(\text{bpy})_2\text{Zn}]^{2+}$) and ligand loss (e.g., $[\text{bpyH}]^+$ and $[2a] \text{H}^+$) are evident in the mass spectrum. The UV-vis spectrum of **4** in dry CH_3CN , and

1 : 1 DMSO : TRIS and 1 : 1 DMSO : PBS at $\text{pH} = 7.4$, are shown in Fig. 6(b). The DMSO : buffer solutions show features consistent with the presence of neutral and anionic forms of **2a**. The emission spectra of **4** ($\lambda_{\text{ex}} = 410 \text{ nm}$; Fig. 6(c)) in 1 : 1 DMSO : TRIS and 1 : 1 DMSO : PBS at $\text{pH} = 7.4$ confirm the presence of the neutral flavonol. Excitation at 480 nm (Fig. 6(d)) produces an emission feature at $\sim 554 \text{ nm}$ in 1 : 1 DMSO : TRIS and $\sim 603 \text{ nm}$ in 1 : 1 DMSO : PBS. The differences in these spectra are indicative of the presence of zinc-coordinated $2a^-$ and free $2a^-$ anion, respectively. The attribution of the emission at $\sim 563 \text{ nm}$ to Zn(II) coordinated $2a^-$ is made on the basis of prior studies.⁴⁴ These results indicate that the zinc ion stays associated with the $2a^-$ anion in 1 : 1 DMSO : TRIS at $\text{pH} = 7.4$, but is displaced from the zinc center in 1 : 1 DMSO : PBS at the same pH.

Effects of surfactants

The flavonol **2a** exhibits low solubility in PBS buffer in the presence of low amounts of DMSO ($\sim 3\%$). This is evident in the lack of a flavonol emission feature of a solution of this composition and observed precipitation. However, in 1 : 1 DMSO : buffer, **2a** is soluble. In order to minimize the amount of DMSO present and gain insight into how the solubility of **2a** may be impacted by interactions with other biomolecules or charged species, we have investigated the solution spectroscopic properties of **2a** in the presence of surfactants. In the presence of the cationic surfactant CTAB (centrimonium bromide), compound **2a** exhibits absorption and emission spectra consistent with the presence of a mixture of **2a** and $2a^-$ (Fig. 7). The emission features associated with these species increase in intensity with increasing CTAB concentration (Fig. 7(b) and (c)), which is similar to studies involving 3-hydroxyflavone.⁵³

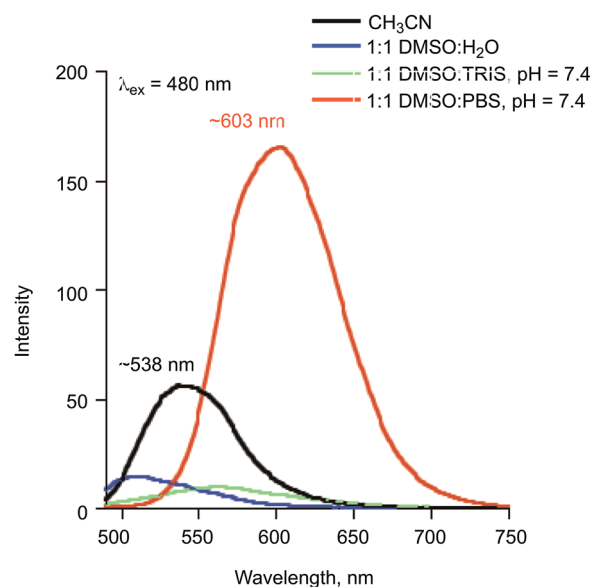


Fig. 5 Emission spectra ($\lambda_{\text{ex}} = 480 \text{ nm}$) of solutions of **2a** (0.10 mM). The emission feature for **2a** at $\sim 538 \text{ nm}$ in CH_3CN is attributed to the neutral flavonol.



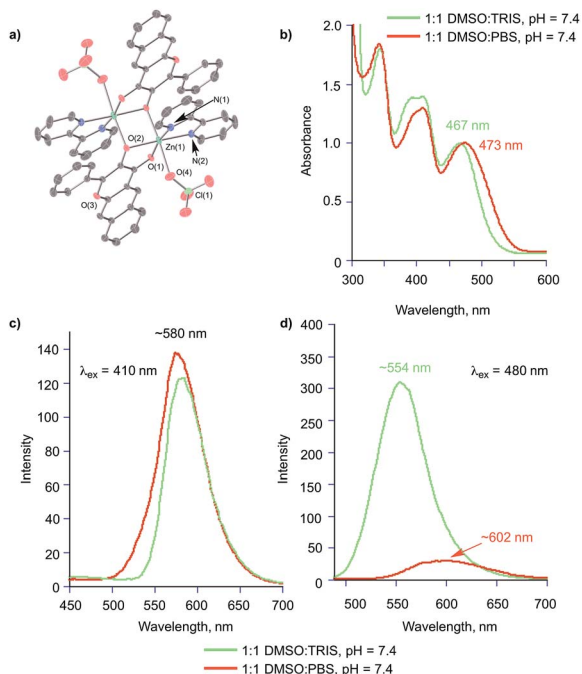


Fig. 6 (a) Thermal ellipsoid representation (50% ellipsoids) of the binuclear structure of **4**. (b) Absorption spectra of **4** (0.10 mM) in 1 : 1 DMSO : TRIS and 1 : 1 DMSO : PBS at pH = 7.4. (c) Emission spectra produced with $\lambda_{\text{ex}} = 410$ nm. (d) Emission spectra produced with $\lambda_{\text{ex}} = 480$ nm.

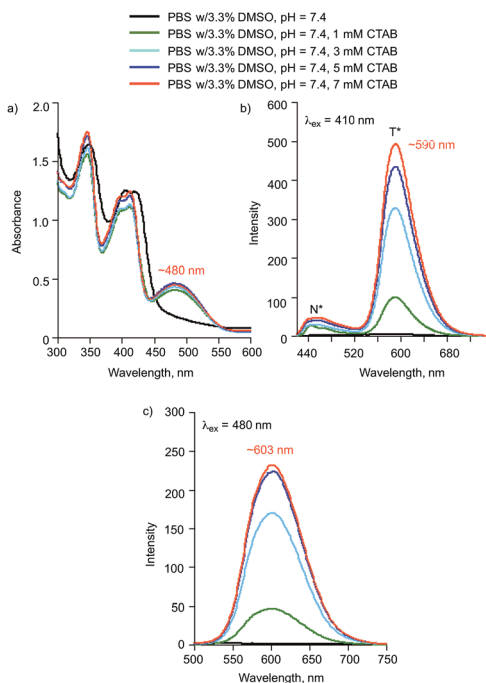


Fig. 7 (a) Absorption spectra of **2a** (0.10 mM) in the presence of various concentrations of CTAB. (b) Emission spectra produced with $\lambda_{\text{ex}} = 410$ nm. (c) Emission spectra produced with $\lambda_{\text{ex}} = 480$ nm.

In the presence of sodium dodecyl sulphate (SDS), the absorption and emission features of **2a** are consistent with the presence of only the neutral form of the flavonol (Fig. 8). This is

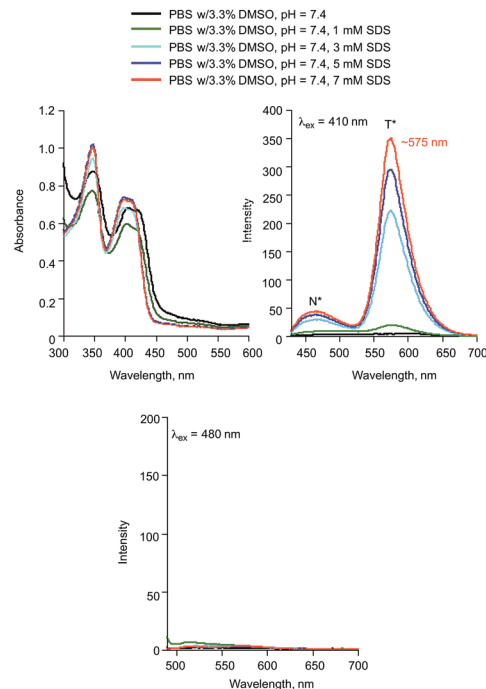


Fig. 8 (a) Absorption spectra of **2a** (0.10 mM) in the presence of various concentrations of SDS. (b) Emission spectra produced with $\lambda_{\text{ex}} = 410$ nm. (c) Emission spectra produced with $\lambda_{\text{ex}} = 480$ nm.

particularly evident in the lack of an emission feature upon excitation at 480 nm.

Serum albumins

Several studies of the binding properties of flavonols to serum albumin proteins using fluorescence spectroscopy have been previously reported.^{54–62} In the case of **2a**, we selectively examined the fluorescence properties of both the flavonol and the tryptophan residues of the protein to probe the **2a**/albumin interaction. Addition of aliquots of BSA to the flavonol in TRIS : DMSO (96 : 4% v:v, pH = 7.4) results in a saturable increase in the intensity of the flavonol T* emission band (Fig. 9). A bathochromic shift (~ 30 nm) of this emission is observed. We note that a similar red shift of the tautomer fluorescence band was identified for 3-hydroxyflavone (3-HfH) upon binding to BSA.⁵⁴ Notably, the emission maximum observed for **2a** in the presence of BSA matches that found in a polar aprotic organic solvent (*e.g.*, CH₃CN (Fig. 4)) wherein the ESIPT process is efficient. This suggests a hydrophobic binding site for the flavonol within the protein environment. As shown in Fig. 10, addition of **2a** to BSA in TRIS : DMSO (96 : 4% v:v, pH = 7.4) results in a decrease of the 340 nm intrinsic emission ($\lambda_{\text{ex}} = 282$ nm) associated with the tryptophan residues of the protein. This quenching suggests that **2a** binds in close proximity to the tryptophan residues (positions 134 and 213). Notably, similar quenching is seen upon titration of human serum albumin (HSA), which contains a single tryptophan residue at position 214 in subdomain IIA of the protein (Fig. S3†). For each protein, the Stern–Volmer equation (eqn (1))



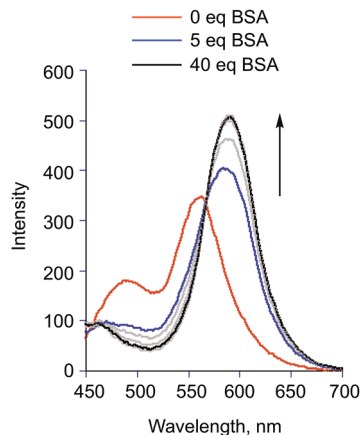


Fig. 9 Emission features of **2a** (1.4 μM) upon addition of increasing amounts of BSA in TRIS : DMSO (96 : 4% v:v, pH = 7.4). $T = 293\text{ K}$, $\lambda_{\text{ex}} = 410\text{ nm}$.

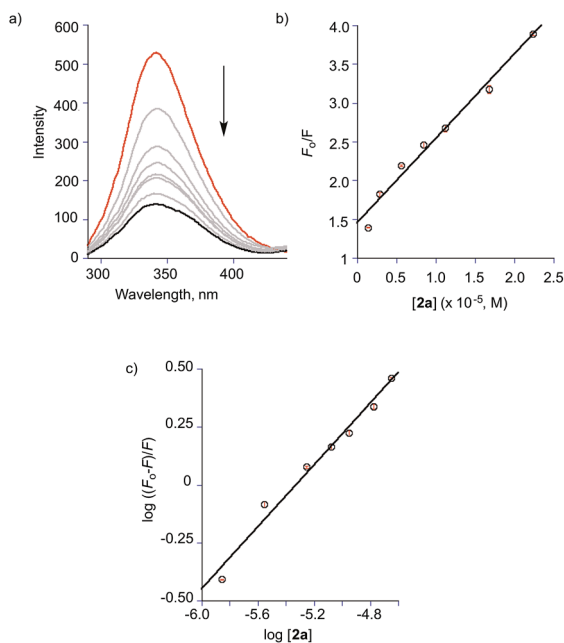


Fig. 10 (a) Fluorescence emission spectra of BSA (1.4 μM) in the presence of various concentrations of **2a** in TRIS/NaCl : DMSO (96 : 4% v:v, pH = 7.4); $T = 298\text{ K}$, $\lambda_{\text{ex}} = 282\text{ nm}$. $[\mathbf{2a}] = 0, 1.4, 2.8, 5.6, 8.4, 11.2, 16.8, \text{ and } 22.4\ \mu\text{M}$. (b) Stern–Volmer plot of data for titration of BSA with **2a**. (c) Modified Stern–Volmer plot of data for titration of BSA with **2a**.

was used to classify the type of fluorescence quenching induced by **2a** as static or dynamic.⁵⁴

$$\frac{F_0}{F} = 1 + k_q \tau_0 [Q] = 1 + K_{\text{sv}} [Q] \quad (1)$$

In this equation, F_0 and F are the fluorescence intensities in the absence and presence of the quencher (**2a**), respectively; k_q is the bimolecular quenching constant, τ_0 is the lifetime of the fluorophore in the absence of quencher (10^{-8} s), $[Q]$ is the

concentration of the quencher and K_{sv} is the Stern–Volmer bimolecular quenching constant.⁵⁴ The Stern–Volmer plot for the titration of BSA with **2a** is shown in Fig. 10(b). As k_q ($1.1 \times 10^{13}\text{ M}^{-1}\text{ s}^{-1}$) is much larger than $2 \times 10^{10}\text{ M}^{-1}\text{ s}^{-1}$ (the maximum diffusion collision quenching rate constant of various quenchers with the biopolymer), it is likely that the quenching in this case is static in nature.⁵⁴ The binding constant K_a and number of binding sites n were calculated from the modified Stern–Volmer plot (Fig. 10(c)) for the titrations of BSA with **2a** according to eqn (2):

$$\log\left(\frac{F_0 - F}{F}\right) = \log K_a + n \log [Q] \quad (2)$$

where $[Q]$ is **2a**. A plot of $\log((F_0 - F)/F_0)$ versus $\log [Q]$ yields $\log K_a$ as the intercept and n as the slope (Fig. 10(c)). The binding constant K_a and binding sites n for **2a** with BSA and HSA are listed in Table 1. Notably, only one equivalent of **2a** binds to BSA and HSA versus two equivalents of the structurally similar but smaller 3-hydroxyflavone (3-HflH).^{54,55} The binding constant for **2a** is ~ 45 -fold lower than that of 3-HflH and is also significantly lower than that of hydroxyl-substituted 3-HflH derivatives that are naturally occurring compounds (e.g., quercetin and morin; Table 1).

Most drug molecules bind to BSA in subdomains IIA and IIIA. Site I (subdomain IIA) is where the blood thinner drug warfarin binds whereas Site II (subdomain IIIA) is the location of ibuprofen binding.⁶³ To gain insight into the binding site of **2a** in BSA, displacement studies were performed with warfarin and ibuprofen. Pre-equilibration of a BSA : warfarin (1 : 1) mixture for 1 h followed by titration with **2a** resulted in the loss of tryptophan fluorescence intensity. The binding constant for

Table 1 Binding constants of **2a** and **3a** with serum albumin proteins at 22 °C with comparisons to other flavonols and salicylic acid derivatives

Compound	Binding constant (K_a, M^{-1})	n	Ref.
2a -BSA	3.2×10^3	0.66	This work
2a -BSA (Zn^{2+})	1.9×10^2	0.48	This work
$[(\text{bpy})\text{Zn}(\mathbf{2a}^-)]\text{ClO}_4$	1.0×10^2	0.39	This work
2a -BSA (Ca^{2+})	3.2×10^3	0.71	This work
2a -BSA (Mg^{2+})	2.5×10^3	0.69	This work
2a -BSA (warfarin)	2.8×10^2	0.46	This work
2a -BSA (ibuprofen)	2.5×10^3	0.67	This work
2a -HSA	3.0×10^3	0.7	This work
2a -HSA (warfarin)	2.5×10^3	0.66	This work
2a -HSA (ibuprofen)	3.0×10^3	0.67	This work
3-HflH-BSA	$1.1\text{--}1.3 \times 10^5$	2	54
3-HflH-HSA	$7.2 \times 10^5; 2.5 \times 10^5$	2	55
Quercetin-BSA	3.65×10^7	1.29	56
Quercetin-BSA	1.00×10^5	0.84	57
Quercetin-BSA	4.85×10^5	1.19	58
Quercetin-HSA	2.30×10^4	1.10	58
Morin-HSA	1.13×10^5	1.06	59
3a -BSA	8.5×10^7	1.7	This work
3a -BSA (warfarin)	6.7×10^3	0.9	This work
3a -BSA (ibuprofen)	2.5×10^5	1.2	This work
BSA-aspirin	5.0×10^3	64	



2a determined from this data ($2.8 \times 10^2 \text{ M}^{-1}$; Fig. S4(a)†) is lower than that observed in the absence of warfarin, suggesting competition for the binding site. A similar experiment involving ibuprofen (Fig. S4(b)†) produced almost no change in the binding constant for **2a**, indicating that no binding of this compound occurs in Site II.

To further probe the binding site of **2a** with BSA we performed *in silico* docking studies using AutoDock Vina.⁴⁹ Two different high affinity binding conformations (Fig. 11) were identified near Site I in subdomain IIA. One of these conformations includes hydrogen-bonding interactions involving the ketone moiety of **2a** (Fig. 11(a)). Because these interactions would preclude the formation of the tautomeric excited state form of **2a**, which is observed by fluorescence, the other conformation (Fig. 11(b)) is more likely. In this binding mode, the hydroxyl oxygen atom, which would be deprotonated in the tautomeric form, is stabilized by the presence of multiple hydrogen bonding interactions.

Human serum albumin (HSA) contains only a single tryptophan residue near Site I. The binding properties for **2a** to HSA are similar to that observed for BSA, with a single molecule binding with a binding constant of $3.0 \times 10^3 \text{ M}^{-1}$ (Fig. S3(a–c)†). Warfarin and ibuprofen experiments with **2a** produced a less pronounced effect relative to those observed for BSA (Fig. S5(a) and (b)†), with a modest affect on binding of **2a** only being observed in the presence of warfarin. Overall, these combined results strongly suggest that serum albumin proteins bind **2a** at Site I.

The binding properties of the *O*-benzoysalicylate CO release product **3a** with BSA were also briefly examined. As shown in Fig. 12(a), this molecule also quenches the intrinsic fluorescence of the protein. A modified Stern–Volmer analysis (Fig. 12(c)) revealed that the binding affinity of **3a** to BSA is significantly higher ($K_a \sim 10^7 \text{ M}^{-1}$) than that of **2a**. Two molecules of **3a** bind to BSA. Competitive binding studies performed using warfarin and ibuprofen (Fig. S6†) show significant changes in the binding constant for **3a** in the presence of both of these site markers. Docking of **3a** with BSA resulted in the identification of two binding sites, with the first being Site I in subdomain IIA and the second being a hydrophobic pocket in subdomain IB. As shown in Fig. 13, binding for *O*-benzoysalicylate derivative in Site I, which is likely the higher affinity binding site, involves hydrogen-bonding interactions with two nearby residues (ARG-208, Glu-353). In subdomain IB, which is a secondary binding site for several drugs including AZT,^{65,66} the interactions appear to be exclusively hydrophobic. Overall, the distinctly different serum albumin binding properties of **2a** and **3a** place these compounds near the bookends of the range of many known drug molecules that exhibit binding constants of 10^4 – 10^7 M^{-1} at Site I in HSA.⁶⁵

Our studies with $[(\text{bpy})\text{Zn}(\text{2a}^-)]\text{ClO}_4$ (**4**) demonstrate that Zn^{2+} will form coordination complexes with the anion 2a^- . To examine the effect of metal ions on the protein binding properties of **2a** in aqueous buffer, titrations of solutions of BSA (1.4 μM) containing 150 μM M^{n+} ($\text{M}^{n+} = \text{Mg}^{2+}$, Ca^{2+} , and Zn^{2+}) with **2a** were performed. As shown in Table 1, the presence of Zn^{2+}

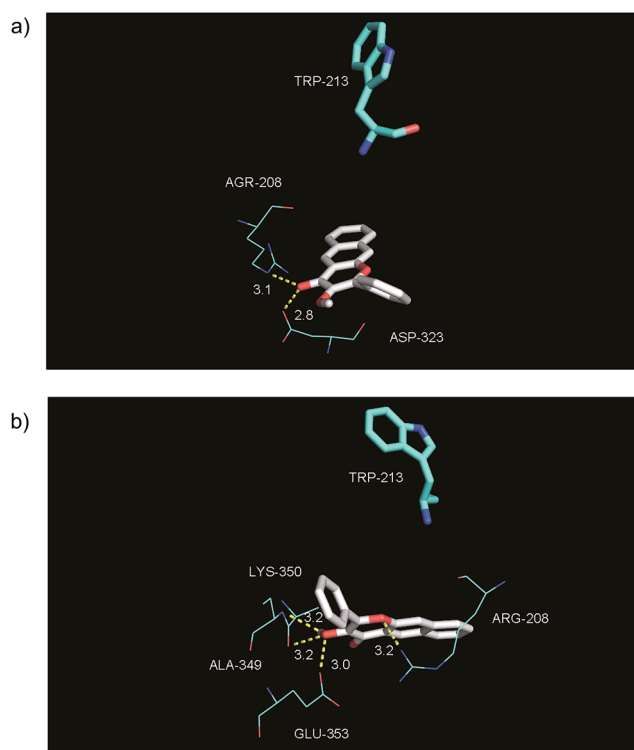


Fig. 11 Views of the binding of **2a** to BSA near Site I in subdomain IIA. Both conformations have similar energies.

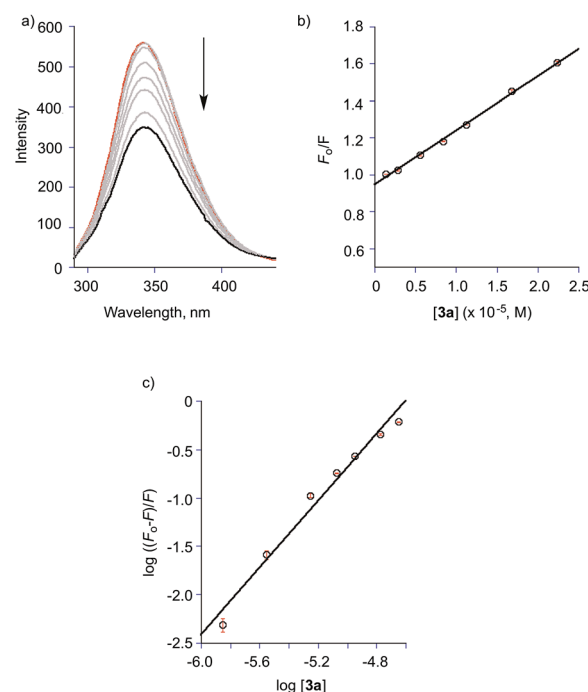


Fig. 12 (a) Fluorescence emission spectrum of BSA (1.4 μM) in presence of various concentrations of **3a** in TRIS buffer at pH = 7.4; $T = 298 \text{ K}$, $\lambda_{\text{ex}} = 282 \text{ nm}$. $[\text{3a}] = 0, 1.4, 2.8, 5.6, 8.4, 11.2, 16.8,$ and $22.4 \mu\text{M}$. (b) Stern–Volmer plot of data for titration of BSA with **3a**. (c) Modified Stern–Volmer plot of data for titration of BSA with **3a**.



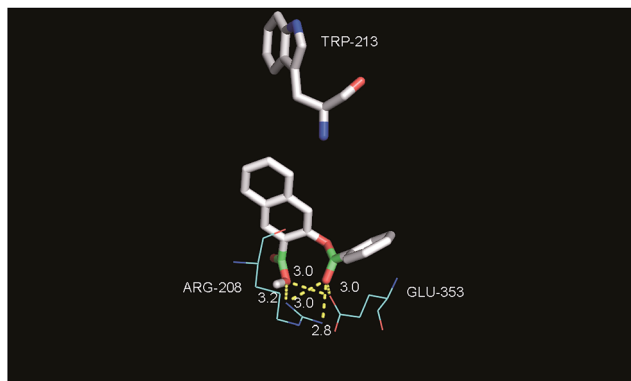


Fig. 13 View of the binding of **3a** to BSA in Site I of subdomain IIA.

Table 2 Quantum yields for visible light ($\lambda = 419$ nm) induced CO release from **2a** under various conditions under air

Conditions (pH = 7.4)	Quantum yield
CH ₃ CN	0.007(3)
1 : 1 DMSO : TRIS	0.006(3)
1 : 1 DMSO : PBS	0.010(3)
4% DMSO : PBS + CTAB	0.0063(1)
BSA (40 eq.) in 3.3% DMSO : TRIS	0.0006(1)
[(bpy)Zn(2a ⁻)]ClO ₄ in 1 : 1 DMSO : H ₂ O	0.017(1)

decreased the binding affinity of **2a** for BSA to a value similar to that observed for the zinc complex [(bpy)Zn(**2a**⁻)]ClO₄ (**4**) (Table 1).

CO release reactivity

With an understanding of the solution properties of **2a** under a variety of aqueous conditions, we next examined the efficiency of the visible light-induced CO release reaction (Scheme 1) under the conditions listed in Table 2. The quantum yields for CO release from **2a/2a**⁻ ranges from 0.006 to 0.010, with binding of **2a** to BSA producing a ~10-fold lower quantum yield than that found for the free molecule in 1 : 1 DMSO : buffer or CH₃CN solutions. Thus the reaction quantum yields found for **2a** do not change appreciably as a function of solvent. This is similar to the quantum yields found for CO release from a Zn(II) 3-hydroxyflavone complex wherein a change of solvent from CH₃CN to H₂O : DMSO (1 : 1) resulted in only a two-fold change in reaction quantum yield.⁶⁷ For **2a**⁻ the presence of Zn²⁺ in the form of the [(bpy)Zn(**2a**⁻)]ClO₄ (**4**) complex produces a slightly higher quantum yield (0.017(1)). We note that the quantum yields for CO release obtained for **2a** under all of these conditions are at least five-fold greater than those of the BODIPY derivatives **1a** and **1b** under aerobic conditions.³⁹

Discussion and conclusions

The development of carbon monoxide releasing molecules (CORMs) for therapeutic applications is an area of significant current interest.^{2-8,15,16} While the majority of CORMs evaluated to

date are based on a metal carbonyl moiety as the CO release unit, challenges regarding incorporation of drug-like structural components, combined with concerns about the possible side reactivity and toxicity of such structures in therapeutic applications, have hampered further development. Metal-free CO-releasing molecules, particularly those that can be controlled in terms of the timing and location of CO release, are attractive as such moieties are likely to be more amenable to standard medicinal chemistry approaches.⁴ In this regard, CO-releasing organic molecules that can be triggered by visible light are of particular current interest. Two novel metal-free, visible light-induced CO release structural motifs have been recently reported. These are based on BODIPY (**1a/1b**)³⁹ and extended flavonol (**2a-d**)⁴²-type structural motifs. Both types of compounds offer attractive features, including low-to-medium toxicity and strong fluorescent emission features that enable tracking in a biological environment. An additional advantage of the BODIPY-based compounds is the structural tunability that enables the use of light of >700 nm to induce CO release. Weaknesses of the BODIPY motif include the requirement of anaerobic conditions to achieve quantitative CO release and the lack of full characterization and toxicity evaluation of the CO release products. The extended flavonol motif offers several notable features that are desirable toward the further development of visible light induced CO release compounds. We previously reported the structural tunability of the flavonol motif in **2a-d** that enables modulation of the wavelength of light that can be used to induce CO release as well as tune the quantum yield for this reaction.⁴² We discovered that one derivative (**2d**) offers the opportunity to access anaerobic CO release reactivity. Another distinct advantage of the framework in **2a** is the ease of synthesis, which involves a one-pot reaction from commercially available starting materials.

In this contribution, we outline details of the solution properties of **2a** in aqueous buffer environments at physiological pH (7.4) and in the presence of charged or biologically relevant molecules. Our results indicate that **2a** can undergo partial ionization to **2a**⁻ under certain conditions (*e.g.*, in PBS buffer or in the presence of a cationic surfactant). We have found that the presence of Zn²⁺ will enhance the quantum yield for CO release from **2a**. Overall this knowledge is important with regard to using **2a** in biological environments.

As we have described herein, compound **2a** is the most reactive metal-free photoCORM motif reported to date under a variety of conditions. The ease of synthesis and structural modification of the extended flavonol framework of **2a**, coupled with the reliability of the molecule in terms of visible light induced CO release reactivity under aqueous conditions, makes it especially well-suited for the further development of a family of CO-releasing molecules with modifications to enhance biological properties, functionality, and targeting. Such efforts are currently underway in our laboratory.

Acknowledgements

We thank the US National Science Foundation (CHE-1301092 to LMB; CHE-1429195 for Bruker Avance III HD Ascend-500 spectrometer) for funding.



References

- G. Kikuchi, T. Yoshida and M. Noguchi, *Biochem. Biophys. Res. Commun.*, 2005, **338**, 558.
- R. Motterlini and L. E. Otterbein, *Nat. Rev. Drug Discovery*, 2010, **9**, 728.
- C. Steiger, C. Hermann and L. Meinel, *Eur. J. Pharm. Biopharm.*, 2016, DOI: /10.1016/j.ejpb.2016.11.002.
- X. Ji, K. Damera, Y. Zheng, B. Yu, L. E. Otterbein and B. Wang, *J. Pharm. Sci.*, 2016, **105**, 406.
- C. Szabo, *Nat. Rev. Drug Discovery*, 2016, **15**, 185.
- K. Nakahira and A. M. K. Choi, *Am. J. Physiol.: Lung Cell. Mol. Physiol.*, 2015, **309**, L1387.
- O. Sulaieva and J. L. Wallace, *Curr. Opin. Pharmacol.*, 2015, **25**, 1.
- C. C. Ramão, W. A. Blattler, J. D. Seixas and G. J. L. Bernardes, *Chem. Soc. Rev.*, 2012, **41**, 3571.
- A. Belhaj, Role of Carbon Monoxide in the Ex Vivo Lung Perfusion Reconditioning, in *ClinicalTrials.Gov*, University Hospital of Mont-Godinne, National Library of Medicine (US), Bethesda (MD), 2014, present. NLM Identifier: NCT02032082.
- I. O. Rosas, Study of Inhaled Carbon Monoxide to Treat Idiopathic Pulmonary Fibrosis, in *ClinicalTrials.Gov*, National Library of Medicine (US), Bethesda (MD), 2010, present. NLM Identifier: NCT01214187.
- Weill Medical College of Cornell University, Safety Study of Inhaled Carbon Monoxide to Treat Acute Respiratory Distress Syndrome (ARDS), in *ClinicalTrials.Gov*, National Library of Medicine (US), Bethesda (MD), 2015, present. NLM Identifier: NCT02425579.
- Medical University of South Carolina, Carbon Monoxide Saturated Medium for Islet Isolation, in *ClinicalTrials.Gov*, National Library of Medicine (US), Bethesda (MD), 2015, present. NLM Identifier: NCT02567240.
- R. Machado, Carbon Monoxide Therapy for Severe Pulmonary Arterial Hypertension (CO in PAH), in *ClinicalTrials.Gov*, University of Illinois at Chicago, National Library of Medicine (US), Bethesda (MD), 2012, present. NLM Identifier: NCT01523548.
- C. Wang, Daping Hospital and the Research Institute of Surgery of the Third Military Medical University, The Safety and Adverse Reaction Study of Neonatal to Inhaled Carbon Monoxide (CO), in *ClinicalTrials.Gov*, National Library of Medicine (US), Bethesda (MD), 2013, present. NLM Identifier: NCT01818843.
- F. Zobi, *Future Med. Chem.*, 2013, **5**, 175.
- U. Schatzschneider, *Br. J. Pharmacol.*, 2015, **172**, 1638.
- B. E. Mann, *Top. Organomet. Chem.*, 2010, **32**, 247.
- I. Chakraborty, S. J. Carrington and P. K. Mascharak, *Acc. Chem. Res.*, 2014, **47**, 2603.
- M. A. Gonzales and P. K. Mascharak, *J. Inorg. Biochem.*, 2014, **133**, 127.
- S. J. Carrington, I. Chakraborty and P. K. Mascharak, *Dalton Trans.*, 2015, **44**, 13828.
- R. Mede, M. Klein, R. A. Claus, S. Kriek, S. Quickert, H. Görls, U. Neugebauer, M. Schmitt, G. Gessner, S. H. Heinemann, J. Popp, M. Bauer and M. Westerhausen, *Inorg. Chem.*, 2016, **55**, 104.
- R. Mede, J. Traber, M. Klein, H. Görls, G. Gessner, P. Hoffmann, M. Schmitt, J. Popp, S. H. Heinemann, U. Neugebauer and M. Westerhausen, *Dalton Trans.*, 2017, **46**, 1684.
- M. Tinajero-Trejo, N. Rana, C. Nagel, H. E. Jesse, T. W. Smith, L. K. Wareham, M. Hippler, U. Schatzschneider and R. K. Poole, *Antioxid. Redox Signaling*, 2016, **24**, 765.
- A. E. Pierri, A. Pallaoro, G. Wu and P. C. Ford, *J. Am. Chem. Soc.*, 2012, **134**, 18197.
- M. A. Wright and J. A. Wright, *Dalton Trans.*, 2016, **45**, 6801.
- E. Stamellou, D. Storz, S. Botov, E. Ntasis, J. Wedel, S. Sollazzo, B. K. Krämer, W. van Son, M. Seelen, G. H. Schmalz, A. Schmidt, M. Hafner and B. A. Yard, *Redox Biol.*, 2014, **2**, 739.
- S. Romanski, E. Stamellou, J. T. Jaraba, D. Storz, B. K. Krämer, M. Hafner, S. Amslinger, H. G. Schmalz and B. A. Yard, *Free Radical Biol. Med.*, 2013, **65**, 78.
- S. Romanski, B. Kraus, M. Guttentag, W. Schlundt, H. Rücker, A. Adler, J. M. Neudörfl, R. Alberto, S. Amslinger and H. G. Schmalz, *Dalton Trans.*, 2012, **41**, 13862.
- S. Romanski, B. Kraus, U. Schatzschneider, J. M. Neudörfl, S. Amslinger and H. G. Schmalz, *Angew. Chem., Int. Ed.*, 2011, **50**, 4038.
- H. Meyer, M. Brenner, S. P. Höfert, T.-O. Knedel, P. C. Kunz, A. M. Schmidt, A. Hamacher, M. U. Kassack and C. Janiak, *Dalton Trans.*, 2016, **45**, 7605.
- P. C. Kunz, H. Meyer, J. Barthel, S. Sollazzo, A. M. Schmidt and C. Janiak, *Chem. Commun.*, 2013, **49**, 4896.
- H. Meyer, F. Winkler, P. Kunz, A. M. Schmidt, A. Hamacher, M. U. Kassack and C. Janiak, *Inorg. Chem.*, 2015, **54**, 11236.
- T. Santos-Silva, A. Mukhopadhyay, J. D. Seixas, G. J. L. Bernardes, C. C. Romão and M. J. Romão, *J. Am. Chem. Soc.*, 2011, **133**, 1192.
- M. Chaves-Ferreira, I. S. Albuquerque, D. Matak-Vinkovic, A. C. Coelho, S. M. Carvalho, L. M. Saraiva, C. C. Ramão and G. J. L. Bernardes, *Angew. Chem., Int. Ed.*, 2015, **54**, 1172.
- A. A. Petruk, A. Vergara, D. Marasco, D. Bikiel, F. Doctorovich, D. A. Estrin and A. Merlino, *Inorg. Chem.*, 2014, **53**, 10456.
- J. D. Seixas, A. Mukhopadhyay, T. Santos-Silva, L. E. Otterbein, D. J. Gallo, S. S. Rodrigues, B. H. Guerreiro, A. M. L. Goncalves, N. Penacho, A. R. Marques, A. C. Coelho, P. M. Reis, M. J. Romão and C. C. Romão, *Dalton Trans.*, 2013, **42**, 5985.
- X. Ji, C. Zhou, K. Ji, R. E. Aghoghovbia, Z. Pan, V. Chittavong, B. Ke and B. Wang, *Angew. Chem., Int. Ed. Engl.*, 2016, **55**, 15846.
- D. Z. Wang, E. Viennois, K. Ji, K. Damera, A. Draganov, Y. Q. Zheng, C. Dai, D. Merlin and B. Wang, *Chem. Commun.*, 2014, **50**, 15890.



- 39 E. Palao, T. Slanina, L. Muchová, T. Solomek, L. Vitek and P. Klán, *J. Am. Chem. Soc.*, 2016, **138**, 126.
- 40 P. Peng, C. Wang, Z. Shi, V. K. Johns, L. Ma, J. Oyer, A. Copik, R. Igarashi and Y. Liao, *Org. Biomol. Chem.*, 2013, **11**, 6671.
- 41 L. A. P. Antony, T. Slanina, P. Sebej, T. Solomek and P. Klán, *Org. Lett.*, 2013, **15**, 4552.
- 42 S. N. Anderson, J. M. Richards, H. J. Esquer, A. D. Benninghoff, A. M. Arif and L. M. Berreau, *ChemistryOpen*, 2015, **4**, 590.
- 43 S. Fetzner, *Appl. Environ. Microbiol.*, 2012, **78**, 2505.
- 44 S. N. Anderson, M. T. Larson and L. M. Berreau, *Dalton Trans.*, 2016, **45**, 14570.
- 45 Y. A. Dávila, M. I. Sancho, M. C. Almandoz and S. E. Blanco, *J. Chem. Eng. Data*, 2013, **58**, 1706.
- 46 K. Grubel, S. Saraf, S. N. Anderson, B. J. Laughlin, R. C. Smith, A. M. Arif and L. M. Berreau, *Inorg. Chim. Acta*, 2012, **407**, 91.
- 47 H. J. Kuhn, S. E. Braslavsky and R. Schmidt, *Pure Appl. Chem.*, 2004, **76**, 2105.
- 48 C. G. Hatchard and C. A. Parker, *Proc. R. Soc. London, Ser. A*, 1956, **235**, 518.
- 49 O. Trott and A. J. Olson, *J. Comput. Chem.*, 2010, **31**, 455.
- 50 B. Dick and N. P. Ernstring, *J. Phys. Chem.*, 1987, **91**, 4261.
- 51 R. Lakowicz, *Principles of Fluorescence Spectroscopy*, Kluwer Academic/Plenum Publishers, New York, 2nd edn, 1999.
- 52 S. L. Sorenson, M. Popova, A. M. Arif, and L. M. Berreau, submitted for publication.
- 53 M. Sarkar and P. K. Sengupta, *Chem. Phys. Lett.*, 1991, **179**, 68.
- 54 J. Guharay, B. Sengupta and P. K. Sengupta, *Proteins*, 2001, **43**, 75.
- 55 A. Sytnik and I. Litvinyuk, *Proc. Natl. Acad. Sci. U. S. A.*, 1996, **93**, 12959.
- 56 J. Xiao, M. Suzuki, X. Jiang, X. Chen, K. Yamamoto, F. Ren and M. Xu, *J. Agric. Food Chem.*, 2008, **56**, 2350.
- 57 E.-H. Liu, L.-W. Qi and P. Li, *Molecules*, 2010, **15**, 9092.
- 58 B. Mishra, A. Barik, K. I. Priyadarsini and H. Mohan, *J. Chem. Sci.*, 2005, **117**, 641.
- 59 M.-X. Xie, M. Long, Y. Liu, C. Qin and Y.-D. Wang, *Biochim. Biophys. Acta*, 2006, **1760**, 1184.
- 60 S. Pal and C. Saha, *J. Biomol. Struct. Dyn.*, 2014, **32**, 1132.
- 61 B. Liu, Y. Pang, R. Bouhenni, E. Duah, S. Paruchuri and L. McDonald, *Chem. Commun.*, 2015, **51**, 11060.
- 62 J. Dai, T. Zou, L. Wang, Y. Zhang and Y. Liu, *Luminescence*, 2014, **29**, 1154.
- 63 S. Pal, C. Saha, M. Hossain, S. K. Dey and G. S. Kumar, *PLoS One*, 2012, **7**, e43321.
- 64 A. Sulkowska, B. Bojko, J. Rownicka and W. W. Sulkowski, *Biopolymers*, 2006, **81**, 464.
- 65 K. Yamasaki, V. T. G. Chuang, T. Maruyama and M. Otagiri, *Biochim. Biophys. Acta*, 2013, **1830**, 5435.
- 66 F. Zsila, *Mol. Pharmaceutics*, 2013, **10**, 1668.
- 67 S. N. Anderson, M. Noble, K. Grubel, B. Marshall, A. M. Arif and L. M. Berreau, *J. Coord. Chem.*, 2014, **67**, 4061–4075.

